Summer 8-6-2018

Three dimensional passive localization for single path arrival with unknown starting conditions

Britt Aguda
baguda@uno.edu

Three dimensional passive localization for single path arrival with unknown starting conditions

A Thesis

Submitted to the Graduate Faculty of the
University of New Orleans
in partial fulfillment of the
Requirements for the degree of

Masters of Science
In
Applied Physics

by

Britt Jacob Aguda

B.S. University of New Orleans, 2016

August, 2018

Acknowledgements

First and foremost, I would like to thank God almighty, creator of all things, and his one begotten son, the Lord Jesus Christ. By the grace of God, I have been given countless blessings and opportunities; all of which I am eternally grateful for having in my life.

After God, comes the greatest blessing that any person can ask for; a wonderful family. My mother, Arlene Aguda, has always been an inspiration and a strength in my life. She gave my brother and me unconditional love that would make the angels in heaven jealous. My mother raised me to be an upright and honest man, she fought for my education and she forged the values that define my character. There is no acknowledgement that can be given in this paper that can fully express the gratitude and love that I have for my mother and everything she has done for me.

Furthermore, I would like to thank my father, Stephen Aguda. Since his childhood, my father has had to fight for the wellbeing of his family. Born as the second son, he was forced to leave school in his adolescence to help support his impoverished family. He worked his fingers to the bone at any job he could get. By his own initiative, he decided to pick up the trade of electrician, and began working toward a brighter future. He has taught me things that cannot be taught in textbooks, shown me things that cannot be seen even in the imagination. He stands as undeniable proof that excellence is an award from God, and that through perseverance and faith, all things are possible. I can only hope to live up to the accomplishments of my father and to teach my children as well as he has taught me. Though he would never ask for it, I thank my father for everything that he has done for me and for our family. His entire life he worked for the future of the family, a sacrifice that can never be repaid by any expressions of gratitude. Instead, I can only offer him a humble and sincere thank you.

Additionally, I would like to thank my brother, Benjamin Aguda, Ph.D. My brother and I are close in age and have always been each other's best friend. No matter what trials or tribulations that I faced in life, I always had a brother who supported me and stood up for me every step of the way. We played together, we fought together, we learned together, we cried together, and we got in trouble together. Ultimately, I am extremely thankful to have been blessed with a brother who shares so many interests and who is so supportive.

Family is a term used to describe bloodlines and kinship bonds, however, family can be used to also describe those who God has brought into our lives as close friends. With that I would like to thank the Delatte Family; Ryan and Cindi and their two beautiful children Isabell and Olivia. I have known both Ryan and Cindi since high school, and I cannot even begin to describe all the times that they have been there for me and my family. Hard working, God fearing, honest, and virtuous are just a few of the terms that come to mind when I think of the Delatte Family. I am thankful every day for the people like the Delatte family who are in my life.

Furthermore, I would like to thank my colleagues and the University of New Orleans. Dr. Juliette Ioup is one the most predominant people who I am thankful for in my professional career. It is a common occurrence in the sciences to have gifted scientists who are lacking in their teaching skills. However, Dr. Juliette is most certainly the exception to this trend. Everything from simple algebra to complex wavelet analysis, Dr. Juliette has the ability to teach it in a simple and direct manor. Professional and personable, Dr. Ioup is always willing to help any student with seemingly any problem at any time. I experienced professors at other universities who maintained a very smug and elitist attitude toward the undergraduate students. One of the

biggest things that brought me to the University of New Orleans was the respect and willingness to help that Dr. Juliette showed to her students. I remember one such occurrence where Dr. Juliette dropped everything that she was doing to help a student in need. The student was not in her class, and his questions were boring and intro-level. Without hesitation she not only sat down with the student to tutor him, but she even referenced books that she had in her collection to make sure that the student understood the concepts. As a researcher who plans on a future career in academia, I can only hope that I am able to teach and mentor students in the way that Dr. Juliette taught and mentored me. Thank you Dr. Juliette, I will carry your teachings in my heart and mind for the rest of my life, and hopefully I can touch others' lives the way you have touched my life.

I would also like to pay respects to and thank the late Dr. George Ioup. Dr. George was a hardworking and honest man, as well as a gifted researcher. He mentored me both professionally and personally without hesitation or compensation. His door was always open and he was always willing help. The University, and indeed the world, lost something very precious with Dr. George's passing; we all lost the brilliance and compassion of one of the most extraordinary people I have ever had the pleasure of knowing. While we are still here trying to fill the impossible void left by his passing, I take comfort knowing that he is in a better place, and has taken his place among the other great scientists of history. I am extremely thankful for having the opportunity to know Dr. George both professionally and personally. May God love him, may God bless him, and may God keep him until we are all reunited again.

Additionally, I would like to thank my research team who have patiently helped me develop the concepts presented in this paper. While some have come and gone over the years, their contributions to my work will always be appreciated, and their influence on my character will always persist. While I could write all day about the appreciation I feel for my research group, I am inclined to give special recognition to Kirk Bienvenu. Kirk was paramount in the development of my research and was there for every success and failure. Together, we poked and pried, laughed and cried, and ultimately we were able to overcome seemingly insurmountable problems that we faced in graduate school. Kirk is truly a terrific man who I am eternally grateful for getting to work with and befriend. Thank you Kirk for your friendship and inspiration, as well as your translation of the notation in our materials textbook… I couldn't have done it without you!

Kendall Leftwich is another outstanding member of my research team that has had a tremendous influence on my work. Academically driven and well mannered, Ken has always been a pleasant person to work with and learn from. While our research was not always aligned, I am wholly thankful for Ken and everything he has done for me.

There is a special lady in my life who I can say with all honesty has made my time at UNO both pleasant and unforgettable. I'm speaking of course about the wonderful Mrs. Denise! Both she and her husband, Mr. Bobby are some of the most terrific people I have ever had the pleasure of getting to know. The battler of bureaucracy, Mrs. Denise has always helped me in my school career and as a personal friend. Thank you Mrs. Denise for all you have done over the years!

I would like to thank my undergraduate officemate, Nick Studer, for inspiring me to go into research and for everything that we learned in the LaACES program. In addition, I would also like to thank Mathew Hellmers, Shyla Clark, Stacey Flynn, Mitch Leche, April Sauru, and all of the people who have enriched my undergraduate and graduate careers with their support and friendship.

Table of Contents

List of figures

Nomenclature and Abbreviations

P_{ref}	Reference point of detector pair
d_s	Separation distance of detector pair
τ	Normalized time ratio
θ_z	Zenith angle of incidence
$E_{\%}$	Percent error map for TAZA expression
$\mathbb{e}_\theta$	The average $E_{\%}$ in the direction θ_z
ψ	Upper and lower bound of the zenith angle
$\mathbb{V}$	Conic region of probability
$\mathbb{W}$	Intersecting region of probability

TDoA	Time difference of arrival
TAZA	TDoA approximation of the zenith angle
TCAM	TDoA conic approximation method

Abstract

Introduced in this paper is the time difference of arrival (TDoA) conic approximation method (TCAM), a technique for passive localization in three dimensions with unknown starting conditions. The TDoA of a mutually detected signal across pairs of detectors is used to calculate the relative angle between the signal source and the center point of the separation between the detectors in the pair. The relative angle is calculated from the TDoA using a mathematical model called the TDoA approximation of the zenith angle (TAZA). The TAZA angle defines the opening angle of a conic region of probability that contains the signal source, produced by each detector pair. The intersecting region of probability is determined from the conic regions of probability and represents the volumetric region with the highest probability of containing the signal source. TCAM was developed and tested using synthetic data in a simulated environment.

Keywords: Physics; Signal Processing; Acoustics; Localization; Numerical Analysis and Scientific Computation;

Chapter 1: Introduction

Wave source localization is a complex endeavor with a multitude of practical applications in a variety of fields. In this paper, a new computational method for passive three dimensional localization will be introduced, and the results of simulation testing of this method will also be presented. The introduced method allows for three dimensional localization of a signal with single path detection across multiple detectors and unknown starting conditions. This method can be applied to any type of signal detected, however it was originally developed for marine acoustic applications.

Marine Acoustics

Developmental inspiration for this method came while localizing marine mammals in the Gulf of Mexico as research for the LADC-GEMM consortium. LADC-GEMM's mission is tracking marine mammal recovery after the Deepwater Horizon oil spill. We deployed sets of highly sensitive hydrophones, called EARS, in strategic locations to study sperm whale, beaked whale, and dolphin acoustic signals in the region of the oil spill. Behavioral studies and population density calculations require passive acoustic localization and tracking of the detected signals. The Gulf of Mexico offers a unique environment for passive acoustic localization. Mud floors and varying sea states eliminate the reliability of multipath detections. Furthermore, underwater monitoring has the added complication of being isolated from any electromagnetic waves (US Department of Commerce, 2013) making time synchronization and data transmission very limited.
Localization in this environment requires an understanding of the history of acoustic localization.

History of Acoustic Localization

Acoustic localization was refined for military use in the early 20th century and has roots in human cognition and perception of sound. The ancient Greeks pondered the "there-here" problem, which attempts to examine how the sound of a plucked Lyre in one place (there) can be perceived by a person in another place (here). There was a plethora of explanations to this question raised from many different schools of thought. One proposed explanation involved the opening of a tunnel in the ether that the sound would flow through, while atomists like Democritus and Epicurus believed that sound was a stream of indivisible atoms that contained information. While diligent in their attempts, no cogent theory of sound would emerge until the 19th century.

The 19th century was a time of scientific growth and development in the West. The wave equation had been established by the works of such people as Newton, Bernoulli, D'Alembert, and Lagrange. In 1822 Joseph Fourier published his theorems on heat flow (Fourier, 1822); which were later used by Georg Simon Ohm to develop Ohm's Acoustic Law in 1843 (Ohm,1843). As psychophysics became more popular in the 19th century, researchers applied these new mechanics theorems to human bioacoustic localization. In 1876, John William Strutt, 3rd Baron Rayleigh, 1904 Nobel Laureate, gave his lecture on "Our perception of the direction of a source of sound" (Strutt, 1876) in which he proposed that human sound localization was the result of amplitude differences detected by each ear. However, Strutt had considerable difficulty

localizing low frequency sounds. Later, in 1907, Strutt gave a follow up lecture in which he proposed that the low frequency problems may be caused by a phase difference perceived across the ears. This was an unpopular notion at the time because it conflicted with Ohm's Acoustic Law, which states that the quality of a complex tone depends solely on the number and relative strength of its partial simple tones, and not on their relative phases. The introduction of the telephone receiver enabled experimenters to control the timing of the signal to each ear separately, and led to new experiments in localization. In the 1920's von Hornbostel and Wertheimer (von Hornbostel, Wertheimer,1920), and later Klemm (Klemm,1920), proposed that the intermediate time could be computed from the intermediate phase as a basis for sound localization.

At this time, the world was still recovering from the mechanized warfare of the first World War. Advances in artillery enabled cannons to hit targets at extreme distances, and the need for localizing the cannon shots, also known as artillery sound ranging, was paramount for strategic advantage. During the war, a method was devised that utilized several detectors separated by a few kilometers. All of the detectors were connected to a central signal processing system that analyzed the time difference of arrival of the sound wave across the detectors. The law of cosines was used to form a non-linear system of equations that could be solved to estimate the wave source location. However, the calculations required were often too difficult to perform while maneuvering in a battle. In a 1924 paper by C.V. Drysdale titled *Submarine Signaling and the Transmission of Sound Through Water*, (C.V. Drysdale,1924) examined the acoustic localization techniques developed on land for submarine applications. In his paper, Drysdale pondered various ways to reduce the computation and data requirements of acoustic localization under water. He proposed pairing hydrophones and modelling the TDoA of a mutually detected wave as a hyperbola whose branches account for the possible locations of the wave source, and the asymptotic lines of the branches can be used to approximate the wave source location.

Conception of method

The localization method presented in this paper is expanding on the concepts presented by Drysdale and uses modern computational capabilities to calculate the source of a signal in three dimensions based on passive detection with unknown starting conditions. This new method will use a mathematical model to determine the relative angles between sets of detectors and a detected signal, and then determine the mutual region that has the highest probability of containing the signal origin. The method offers several expressions for computing the relative angles; each having different accuracy and computational requirements. The method accounts for possible error in the mathematical model and applies upper and lower error bounds to the localization algorithm. Ultimately, the method was conceptualized as a fast and affective approach to three dimensional passive localization in order to expedite localization operations in various research fields.

Chapter 2: Methodology

Signal Detector Pairing

The technique introduced here is a method of spatial analysis derived from the time difference of arrival of a signal, TDoA, across at least two detectors. For this paper, the method assumes omnidirectional wave detectors with infinite detection range and perfect time synchronization, as well as a constant wave speed profile; however, the method can be augmented to account for variations in the detector system characteristics. Generally, the technique requires two or more time synchronized detectors positioned in three dimensional space. These detectors do not need to be positioned in any particular orientation, and can be positioned randomly. The detectors are grouped into pairs and analyzed together as a *detector pair*. Any two detectors can be paired, and more pairs result in more accurate localization. The pairs should be chosen based on their proximity and alignment to each other. Consideration of the separation distance with respect to the sampling frequency and wave speed when pairing detectors can reduce error, and careful attention to alignment can simplify the rotations that are needed in the method.

Furthermore, the detectors can be grouped into multiple pairs with multiple other detectors. *Cross-pairing* the detectors in this manner allows for more pairs to contribute to the localization accuracy without the addition of more detectors. The method analyzes each pair individually then cross references the results of each; thus arbitrary pairing of detectors will not affect the behavior of the method.

However, in order to be paired, both hydrophones in the pair must be time synchronized with respect to each other, which can limit the choice of detectors to be paired. In addition, the separation distance between the detectors in a pair must be large enough to allow for accurate signal detection while accounting for wave speed and sampling frequency, which can also limit cross-pairing.

TDoA Approximation of the Zenith Angle

The TDoA Approximation of the Zenith Angle (TAZA) is a mathematical model of the relationship of the Time Difference of Arrival of a detected wave by a detector pair and the zenith angle of the wave to the midpoint half way between the detectors in the pair. The technique normalizes the TDoA by taking the ratio of the detected TDoA and the maximum possible TDoA. The maximum TDoA is determined by the separation distance of the detectors in a pair and the wave speed across the separation distance. Let

$$\Delta t = t_2 - t_1 \qquad \textit{(eq.01)}$$

$$t_{max} = \frac{d_s}{c_w} \qquad \textit{(eq.02)}$$

$$\tau = \frac{\Delta t}{t_{max}}, \qquad -1 \leq \tau \leq 1 \qquad \textit{(eq.03)}$$

where Δt is the TDoA of detection times t_1, for detector 1, and t_2, for detector 2, t_{max} is the maximum possible TDoA, d_s is the distance of separation of the two detectors, c_w is the wave propagation speed, and τ is the normalized time ratio.

The midpoint of the separation distance, called the reference point, P_{ref}, is defined as half of the separation distance in the direction of the second detector from the first detector, as shown in figure 1.

$$P_{ref} = \frac{1}{2} d_s \hat{r}_{12} \qquad \textit{(eq.04)}$$

The first detector, called the reference detector, is defined by the experimenter and allows for standardization of directionality across all detector pairs. The reference point and reference detector define the local Euclidian coordinate system for each detector pair; where P_{ref} defines the origin, and the reference detector is located at half the separation distance in the z direction, $\frac{1}{2} d_s \hat{z}$, thus defining the z-axis, as seen in figure 1.

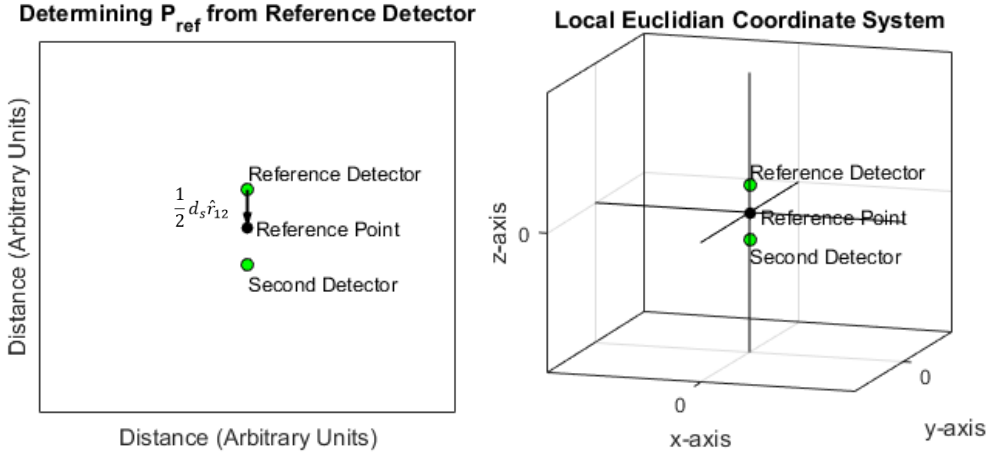

Figure 1: The reference point is determined as half of the separation distance of the pair in the direction from the reference detector to the second detector as defined by eq.04 (left). The reference point now defines the origin of the local Euclidian space around the detector pair with the positive z-axis in the direction of the reference detector (right).

The zenith angle of incidence is defined as the angle from the xy-plane toward the z-axis from the reference point to the detected wave source. Omnidirectional ambiguity and symmetry allows for interchangeability of the x and y axes across all detector pairs so long as handedness is consistent. The arbitrary nature of assigning the x and y axes allows for the problem to be simplified into two dimensions by defining the R-axis as a composite of the x and y axes:

$$\hat{R} = \sqrt{\hat{x}^2 + \hat{y}^2}$$

Where the positive direction of the R-axis is in the direction of the wave source from P_{ref}. While the azimuthal angle is unknown, thus the exact direction of the R-axis is unknown, the zenith angle is the same for all azimuthal values. This allows for the calculations to be simplified into a two dimensional cross section, the R-Z plane, on which both P_{ref} and the wave source must both

be located. On the R-Z plane, the zenith angle of incidence, θ_z, is the angle between the R-axis and the wave source from P_{ref}, as seen in figure 2.

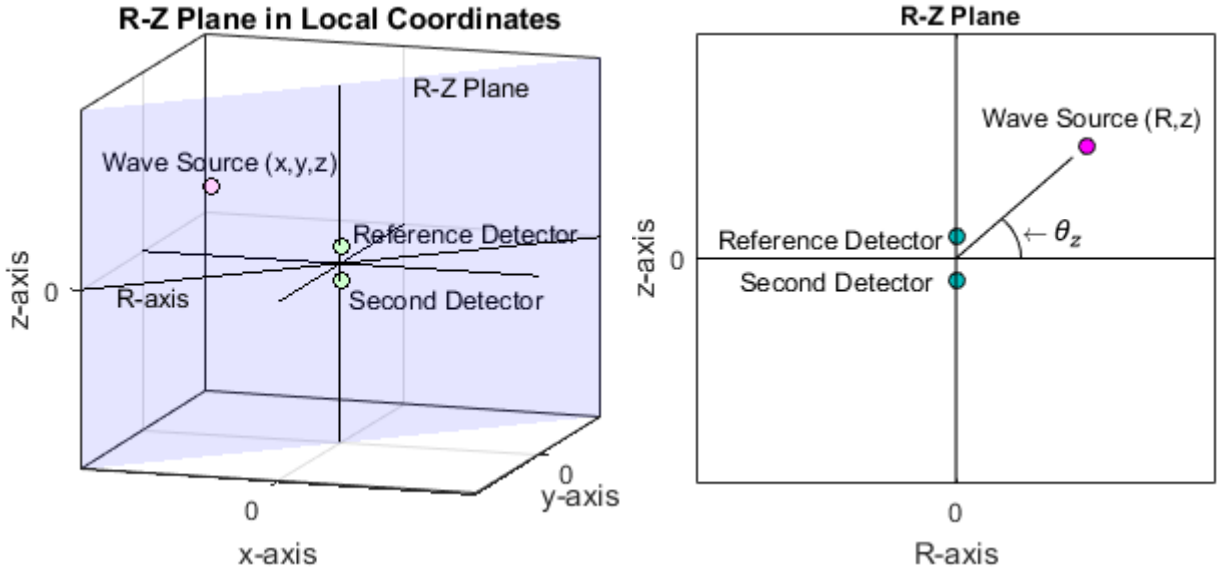

Figure 2: The R-Z plane is a cross section of the local coordinate system on which both P_{ref} and the wave source are located (left). The zenith angle of incidence, θ_z, is shown on the R-Z plane (right).

The dependence of the zenith angle of incidence, θ_z, on the time ratio can be expanded in an n[th]-order polynomial:

$$\theta_z(\tau) = \frac{\tau}{|\tau|} \sum_{i=0}^{n} a_i |\tau|^i \qquad \textit{(eq.05)}$$

where a_i is a weighting coefficient in the series of length $(n+1)$. Error is minimized for a longer series (larger values of n); however, testing shows a value of $n > 50$ is sufficiently accurate and is used as the polynomial order for testing in this work. Mirror symmetry across the xy-plane means that the value of the time ratio will be the same for detections at the same angle both above and below the xy-plane, but they will have opposite signs (the classic ambiguity problem). For this reason, the absolute value of the time ratio is taken for the polynomial and the resultant calculated zenith angle is scaled to have the same sign as the time ratio.

$$\frac{\tau}{|\tau|} = \begin{cases} 1 & \tau > 0 \\ -1 & \tau < 0 \\ 0 & \tau = 0 \end{cases}$$

The polynomial expression for TAZA is highly accurate with many terms, but computing the n^{th}-order polynomial can be difficult for some applications. TAZA can also be modeled as a trigonometric expression that uses only two coefficients b_0 and b_1, but suffers from reduced accuracy:

$$\theta_z(\tau) = \frac{b_0 \tau}{|\tau|} \operatorname{artanh}(b_1 |\tau|) \qquad \textit{(eq.06)}$$

This expression allows for very fast and easy calculations of the zenith angle with reasonable accuracy. The accuracy can be improved by applying a correction factor, Φ_z, which can be modeled as a thirteenth-order polynomial.

$$\Phi_z = 1 - \sum_{h=0}^{13} c_h |\tau|^h \qquad \textit{(eq.07)}$$

Thereby making a sixteen coefficient expression for TAZA:

$$\theta_z(\tau) = \frac{b_0 \tau}{|\tau|} \operatorname{artanh}(b_1 |\tau|) \cdot \Phi_z \qquad \textit{(eq.08)}$$

The fourteen correction factor coefficients, c, plus the two hyperbolic arctangent coefficients, b, gave accuracy comparable to the fiftieth order zenith angle polynomial for the test cases described below.

Figure 3 shows the zenith angle versus the time ratio generated using simulations for the different expressions for the TAZA model. The solid orange line shows the result for a 50 coefficient polynomial expression (eq.05), the solid blue line shows the result for the two coefficient trigonometric expression (eq.06), and the dashed amber line shows the result for the 16 coefficient corrected trigonometric expression (eq.08). The b and c coefficients used are given in table 1; the full table of a_n coefficients can be found in the appendix. It can be seen that the corrected trigonometric expression is nearly identical to the 50 coefficient polynomial expression at this scale, unlike the two-coefficient trigonometric expression which diverges at higher values of τ. However, the ease of calculating the two coefficient trigonometric expression makes it a viable option for fairly accurate results with limited computational resources. Minor differences in the expressions cannot be seen at this scale, however, the accuracy of each expression compared to the true value is illustrated in figure 6. Examining the error of each in figure 6 shows that the 50 coefficient expression is more accurate than the 16 coefficient expression.

b_0	61.20987	c_6	2.43E+05
b_1	0.879179	c_7	-7.13E+05
c_0	-5.59E-02	c_8	1.44E+06
c_1	-8.49E-01	c_9	-2.01E+06
c_2	3.87E+01	c_{10}	1.90E+06
c_3	-7.71E+02	c_{11}	-1.16E+06
c_4	8.41E+03	c_{12}	4.14E+05
c_5	-5.60E+04	c_{13}	-6.54E+04

Table 1: TAZA coefficients b and c for eq.07 and eq.08

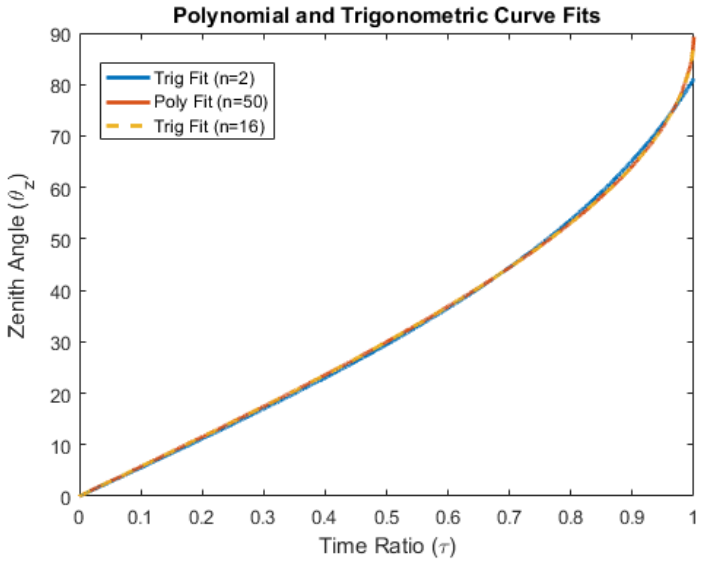

Figure 3: Comparison of the TAZA expressions for the θ_z vs τ relationship. The $n = 50$ and $n = 16$ plots are identical at this scale, while the $n = 2$ plot varies slightly for lower values of τ but diverges for values of $\tau > 0.7$.

Conic Regions of Probability

The approximated zenith angle on the R-Z plane defines a *line of probability* that extends from P_{ref} to the wave source. The line of probability is infinitely long (max detection range) and indicates all of the points in the direction of the angle where wave source could be located. The conic surface of probability is the result of revolving the line of probability by the full range of azimuthal ambiguity of the omnidirectional detectors around the z-axis, and represents the possible locations the source could be located in three dimensions. Earlier, the problem was simplified into two dimensions on the R-Z plane. When expanded back into three dimensions, the rotated line of probability creates a hollow cone whose vertex is located at P_{ref} and whose edges extend to infinity (max detection range) around the local z-axis, as seen in figure 4.

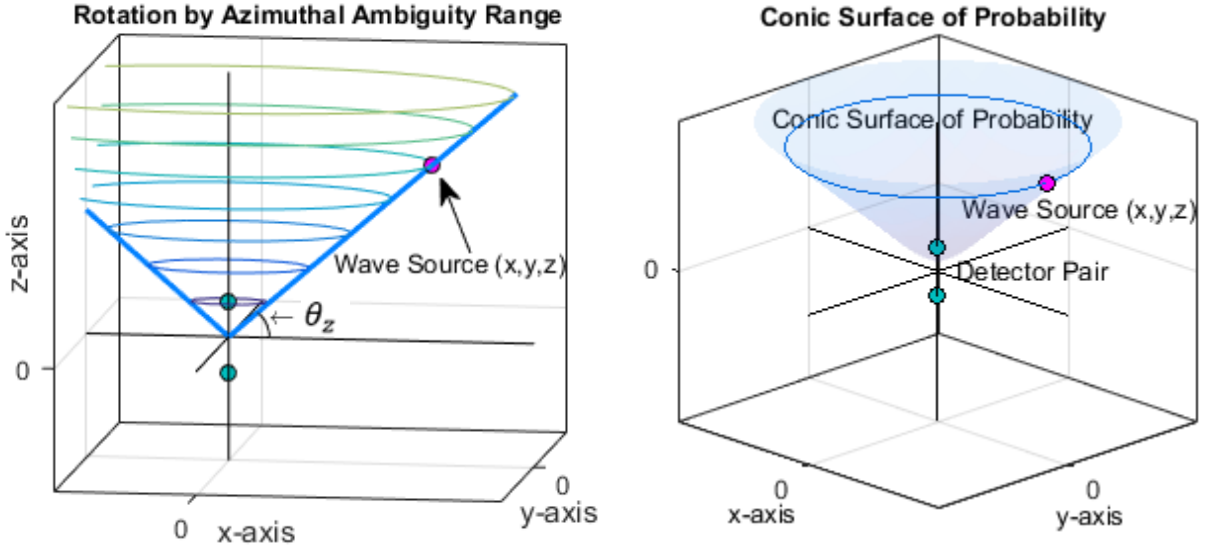

Figure 4: Rotation of the line of probability defined by the TAZA angle, θ_z, by the full range of azimuthal ambiguity (2π) around the z-axis (left) creates a conic surface of probability on which the wave source must be located.

The conic surface of probability, V, is expressed as:

$$V(x, y; \theta_z) = R(x, y) \tan(\theta_z) \qquad \textit{(eq.09)}$$

where,

$$R(x, y) = \sqrt{x^2 + y^2} \qquad \textit{(eq.10)}$$

The conic surface of probability is an ideal estimate of all possible source locations given by the TAZA model. However, the various accuracies for the various equations of TAZA means that the calculated zenith angle represents a center angle with an upper and lower error bounds, $\pm\psi$, in which the wave source must be located, as shown in figure 5.

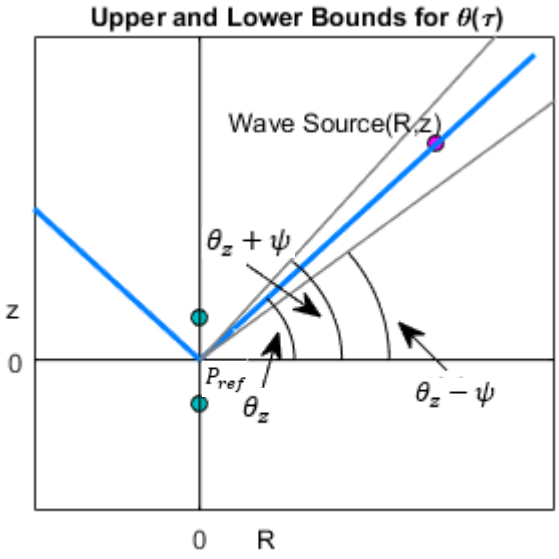

Figure 5: To account for the error in the various equations for TAZA, an upper and lower bound, ψ, on θ_z results in a conic region of probability derived from the expanded conic surface of probability.

The conic surface of probability is expanded into a conic region of probability when the upper and lower bounds are also included in the rotation making a hollow funnel whose walls thicken with distance from the reference point at the conic vertex. The conic region of probability, $\mathbb{V}$, is expressed as

$$\mathbb{V} = \{(x, y, z) \in \mathbb{R}^3 | V(x, y; \theta_z - \psi) \leq z \leq V(x, y; \theta_z + \psi)\} \qquad \textit{(eq.11)}$$

where ψ is the upper and lower bound, measured in degrees, of the zenith angle, described by

$$\psi = \mathbb{e}_\theta + \mathbb{e}_c \qquad \textit{(eq.12)}$$

where the contributions of the error of the TAZA expression used to approximate the zenith angle are given by $\mathbb{e}_\theta$, and the error of the wave speed profile on the detected TDoA to the angle bounds is given by $\mathbb{e}_c$. These bounds also are measured in degrees. The conic region of probability is composed of the region between the upper and lower bounds of the zenith angle. Minimizing the conic region by reducing ψ will result in a more precise localization. The wave speed error, $\mathbb{e}_c$, is modeled for the detection environment for each application. For constant wave speed profiles, $\mathbb{e}_c = 0$.

Each TAZA expression will have a unique error, $\mathbb{e}_\theta$, the average percent error of the expression in the direction of θ_z on the R-Z plane. The percent error, $E_{\%}$, is a scaler field across R and z, expressed as

$$E_{\%}(R(x, y), z) = \frac{\left|\theta_z(\tau) - \arctan\left(\frac{z}{R}\right)\right|}{\arctan\left(\frac{z}{R}\right)} \times 100 \qquad \textit{(eq.13)}$$

The average of $E_{\%}$ in the direction of θ_z is given as

$$\mathbb{e}_\theta = \frac{\theta_z}{100 \int_C dr} \int_C E_{\%}(R(x, y), z)\, dr \;;\quad C = \mathrm{r} \cdot \tan(\theta_z)\Big|_0^\infty \;;\quad r = \sqrt{R^2 + z^2} \qquad \textit{(eq.14)}$$

Due to radial symmetry about the z-axis and mirror symmetry across the xy-plane, $E_{\%}$ is the same for any direction of R; thus allowing for easy two dimensional modelling on the R-Z plane.

Analysis shows a radial trend in $E_{\%}$ from the reference point; as seen in figure 6. Therefore, $\mathbb{e}_\theta$ is taken linearly across C, which is a line mimicking a cross section of V, as illustrated in figure 6.

The $E_{\%}$ for the different expressions for TAZA can be seen in figure 6, as well as a visual representation of the line C along which the average of $E_{\%}$ is calculated. The color scales for each of the three plots in figure 6 illustrate the range of error for each expression, and the average percent error, $\bar{E}_{\%}$, illustrates the overall accuracy of the expression. As expected, all of the expressions have increased $E_{\%}$ for values of θ_z that are closer to zero due to the relative scaling of percentages. Likewise, all of the expressions have increased $E_{\%}$ for values of θ_z close to 90° due to the up-sweeping "hockey stick" trend of the TAZA model for higher values of τ, as seen in figure 3. As discussed, the line C represents the line that $\mathbb{e}_\theta$ is calculated along in the direction of θ_z, visualizations of C are included in figure 6. The radial trend of $E_{\%}$ results in values of $\mathbb{e}_\theta$ that have negligible variance along C. Predictably, each equation for TAZA has different $\mathbb{e}_\theta$ associated for each angle θ_z, as seen in figure 7.

TDoA Conic Approximation Method

The TDoA conic approximation method, or TCAM, utilizes the *conic regions of probability* of multiple detector pairs to determine the *intersecting region of probability* for localization. A signal event detected across n numbers of detector pairs will produce n conic regions of probability in which the wave source must be mutually located. As stated, greater values of n results in more conic regions of probability intersected, which results in greater accuracy. In order to find this intersecting region, all conic regions of probability must be oriented with respect to a common coordinate system.

The n different coordinate systems must be rotated and translated onto a base coordinate system to allow for computation of the intersecting mutual regions in which the wave source is located. One detector pair is chosen by the experimenter as the base pair that defines the base coordinate system. The coordinate systems for the other detector pairs are reoriented with respect to the base coordinate system using rotation and translation matrices. The n^{th} conic region in the base coordinate system is given as:

$$\mathbb{V}'_n = \mathbb{V}_n \lambda_n + T_n \qquad \textit{(eq.15)}$$

Where λ is the rotation matrix that defines the offset of the pair's axes verses the base axes, and T is the translation matrix that relocates the conic region with respect to the base coordinate system's origin. After all of the contributing detector pairs' coordinate systems have been reoriented with respect to the base coordinate system, the intersections of their conic regions of probability can be analyzed to create a three dimensional volumetric estimation of the wave source location, called the *intersecting region of probability*.

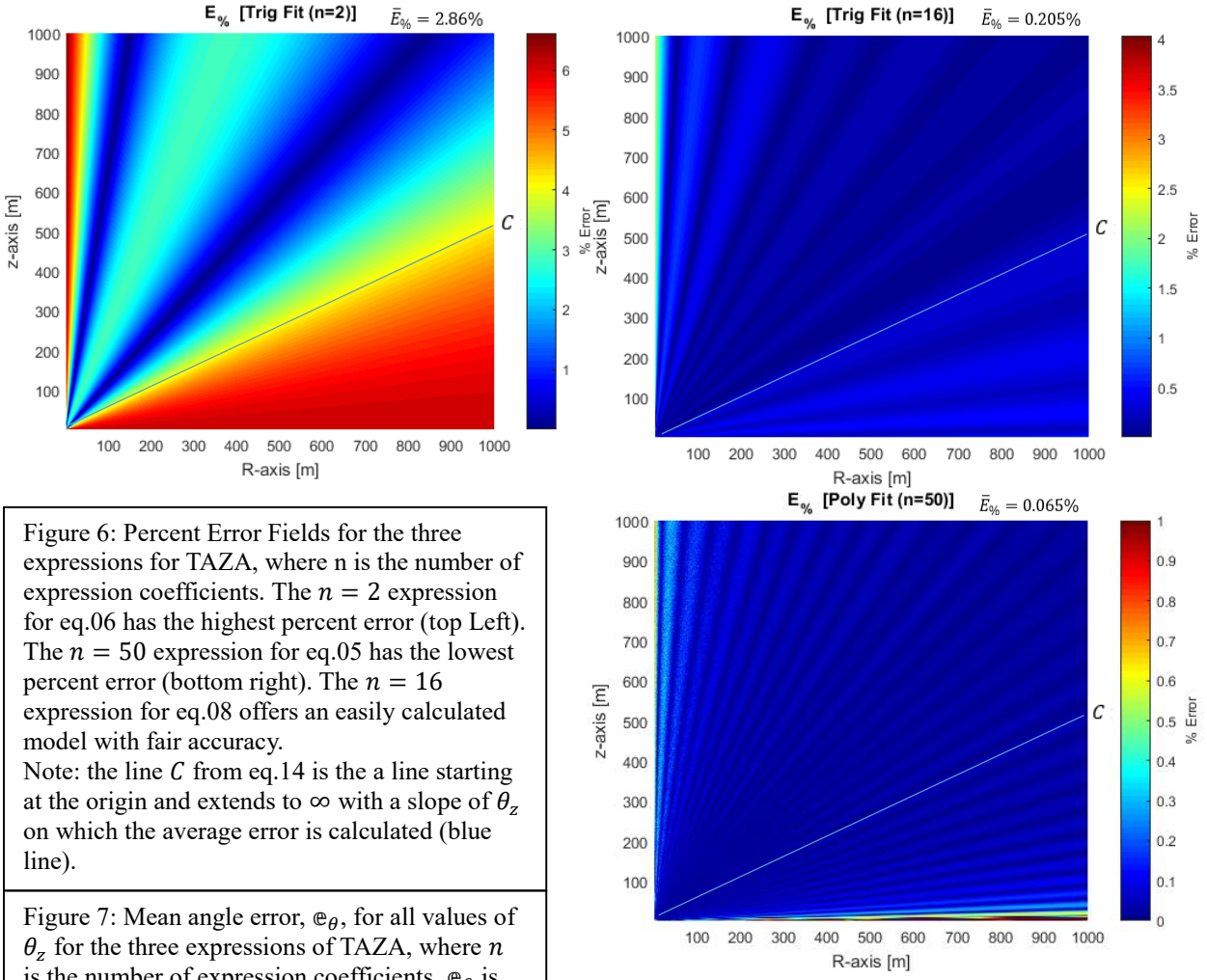

Figure 6: Percent Error Fields for the three expressions for TAZA, where n is the number of expression coefficients. The $n = 2$ expression for eq.06 has the highest percent error (top Left). The $n = 50$ expression for eq.05 has the lowest percent error (bottom right). The $n = 16$ expression for eq.08 offers an easily calculated model with fair accuracy.
Note: the line C from eq.14 is the a line starting at the origin and extends to ∞ with a slope of θ_z on which the average error is calculated (blue line).

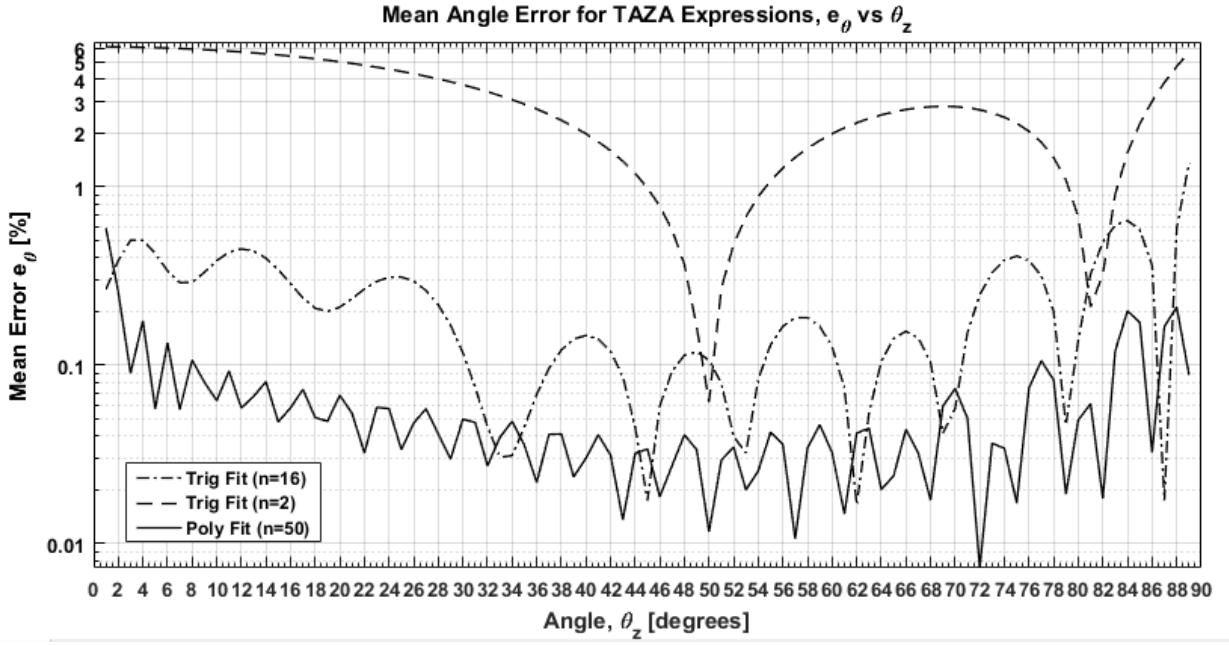

Figure 7: Mean angle error, $\mathbb{e}_\theta$, for all values of θ_z for the three expressions of TAZA, where n is the number of expression coefficients. $\mathbb{e}_\theta$ is given in %, before being scaled by θ_z in eq.14

The *intersecting region of probability*, $\mathbb{W}$, for n detector pairs is expressed as the volume of intersection of the n conic regions of probability in the base coordinate system:

$$\mathbb{W}_n = \{(x,y,z) \in \mathbb{R}^3 | (x,y,z) \in \bigcap_{k=1}^{n} \mathbb{V}'_k\} \qquad \textit{(eq.16)}$$

The mutual region of probability represents the possible locations of the wave source with respect to the base coordinate system. Figure 8 shows a cross section of the volume $\mathbb{W}_n$ on the R-z plane of the base coordinate system with the reoriented $\mathbb{V}'_n$ intersecting with the base region $\mathbb{V}_1$.

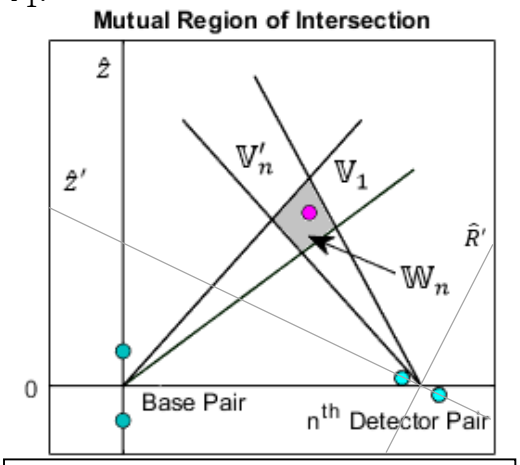

Figure 8: 2D cross section of the intersecting region of probability, $\mathbb{W}$, for two conic regions of probability, $\mathbb{V}$, created by two detector pairs. Shown in the base coordinate system $(\hat{z}, \hat{R})$, with the n^{th}coordinate system $(\hat{z}', \hat{R}')$.

The volume of $\mathbb{W}$ can be narrowed by optimizing ψ, and can be reduced by higher values of n. The probability of source location is evenly distributed at all points in $\mathbb{W}$. If one or more conic regions fail to intersect with the others over its volume, then the probability of the source location presumably will be greater for points closer to the nearest mutual region, or it can simply be disregarded if unneeded. Overall, the TCAM localization technique finds the intersecting region of probability, $\mathbb{W}_n$, of n conic regions of probability, $\mathbb{V}'$, created by n oriented and bound conic surfaces of probability, $V \pm \psi$, determined by the TAZA model's calculation of the zenith angle, θ_z, from the normalized time ratios, τ, across n detector pairs.

Alternatively, TCAM computation can be simplified by using the intersections of the conic surfaces of probability instead of the conic regions of probability. Assuming no angle error allows for calculating the intersections of surfaces instead of volumes. This can be generally expressed as

$$W_n = \{(x,y,z) \in \mathbb{R}^3 | (x,y,z) \in \bigcap_{k=1}^{n} V'_k\} \qquad \textit{(eq.17)}$$

where W_n are the intersections of n conic surfaces of probability. W can be expanded into a volume after calculation to account for possible error since W is always the center of $\mathbb{W}$. The expansion expression can be modeled as a volume around W that extends outward in every direction by radius, r_ψ, that depends on ψ and the separation distance, d_r, of W and P_{ref}:

$$r_\psi = \psi \cdot d_r \qquad \textit{(eq.18)}$$

This method offers a second, less computationally heavy, approach to TCAM localization.

Chapter 3: Localization Results

The TCAM technique was developed using geometric deduction and computational simulations, and was tested using synthetic data. The technique was able to efficiently localize the simulated wave source in three dimensions into a volumetric region of probability. The size and shape of the region depends on the number and orientation of the contributing detector pairs. All simulations excluded possible multipath arrivals, assumed perfect detector synchronization and sampling, assumed infinite detection range with no wave attenuation, assumed a constant wave speed profile of 1500 $\frac{m}{s}$ (emulative of underwater acoustics), and disregarded non-intersecting conic regions. The TAZA expression given in eq.05 is used for all calculations and ψ is assumed to be 0.1° for visualization purposes.

In this chapter, the results of the TCAM technique for localizing signal sources in the simulated three dimensional space are analyzed. The results of localizing with up to four detector pairs will be presented as well as demonstrations of cross-pairing. The simulations cover examples of when the detectors are in a fixed arrangement with each other as well as when the detectors are at randomized locations. All of the presented signal source locations were randomly generated independently from the localization algorithm.

The figures presented in this chapter follow a general format where the localization results for a single detection is shown from four different viewpoints. Due to the difficulty of visualizing volumetric data in three dimensional space, each figure includes a 3D view (top left), a top-down view down z-axis (top right), a side view down the x-axis (bottom left), and a side view down the y-axis (bottom right). Each figure in this chapter will also include a legend for all plots in the figure as well as details of the trial in the figure title. The visual representation of the intersecting volume will change depending on the size of the volume. Smaller volumes are difficult to see at scale; thus larger markers are used for the smaller volumes. Furthermore, each detector is uniquely color coded in each figure. The color of each detector carries over to each plot inside of the figure allowing for easy visualization of which detector is where in the rotated visual representations of the figures. The color assignments are unique to each figure, and do not persist from figure to figure. Furthermore, the

Localization with two detectors

Locating fixed sources with a single detector pair is the most straight forward and least accurate example of TCAM. Only one detector pair results in one conic region of probability, thus the intersecting region of probability is the same as the conic region of probability, as seen in figure 9. While a single conic region of probability doesn't offer much precision, it does accurately contain the signal source location and provides a broad estimate for localization. If only one detector pair is contributing to the calculation, then it will indubitably be the base pair; however, it can still be reoriented to another base coordinate system if needed for a specific application.

Furthermore, figure 9 offers a good visualization of the conic regions in simulated three dimensional space. The small value of ψ results in a fairly narrow conic region; the thickness of the region can easily be seen in the two top plots of figure 9.

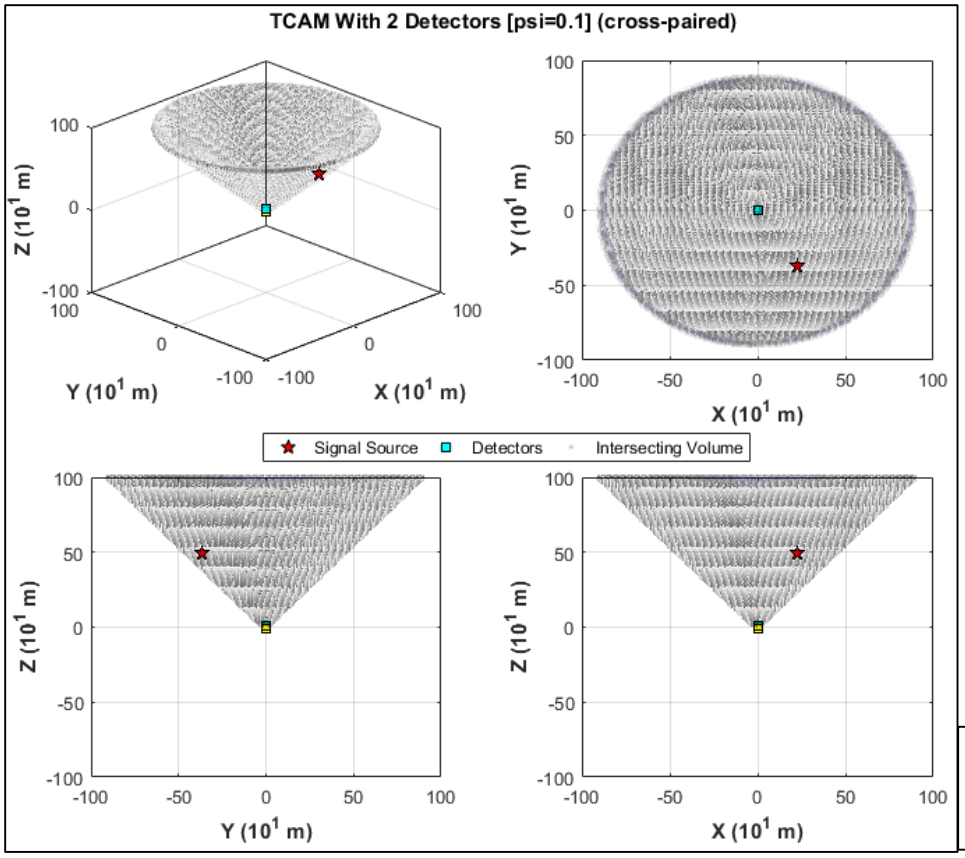

Figure 9:
TCAM results for 2 detectors.

Localization with four detectors

The addition of another detector pair allows for the intersection of the conic regions of probability to be determined. Generally, the intersecting region of two conic regions is a non-uniform hyperbolic paraboloid toroidal volume that snakes through the local space as seen in figure 10. This tubular volume offers a much more precise localization estimate, but it still leaves a considerable amount of ambiguity as to the signal's actual origin. The detectors in figure 10 are arranged randomly in the simulated space, and are arbitrarily paired. This haphazard detector arrangement creates the twisted and crooked non-uniform shape of the hyperbolic paraboloid toroidal volume that is shown in figure 10.

The accuracy of localization is greatly improved by cross-pairing the same arrangement of detectors as seen in figure 11. The volumetric results of figure 10 are caused by the low number of conic regions contributing to the calculation. Cross-pairing the detectors to every possible permutation allows for more conic regions to contribute without having to increase the number of detectors. It can be seen by comparing figure 10 and figure 11 that cross-pairing can greatly improve the precision of TCAM if the conditions of the experiment allow for cross-pairing. As previously stated, cross-pairing requires ideal conditions that include detector separation distances, detector synchronization, and wave speed profile.

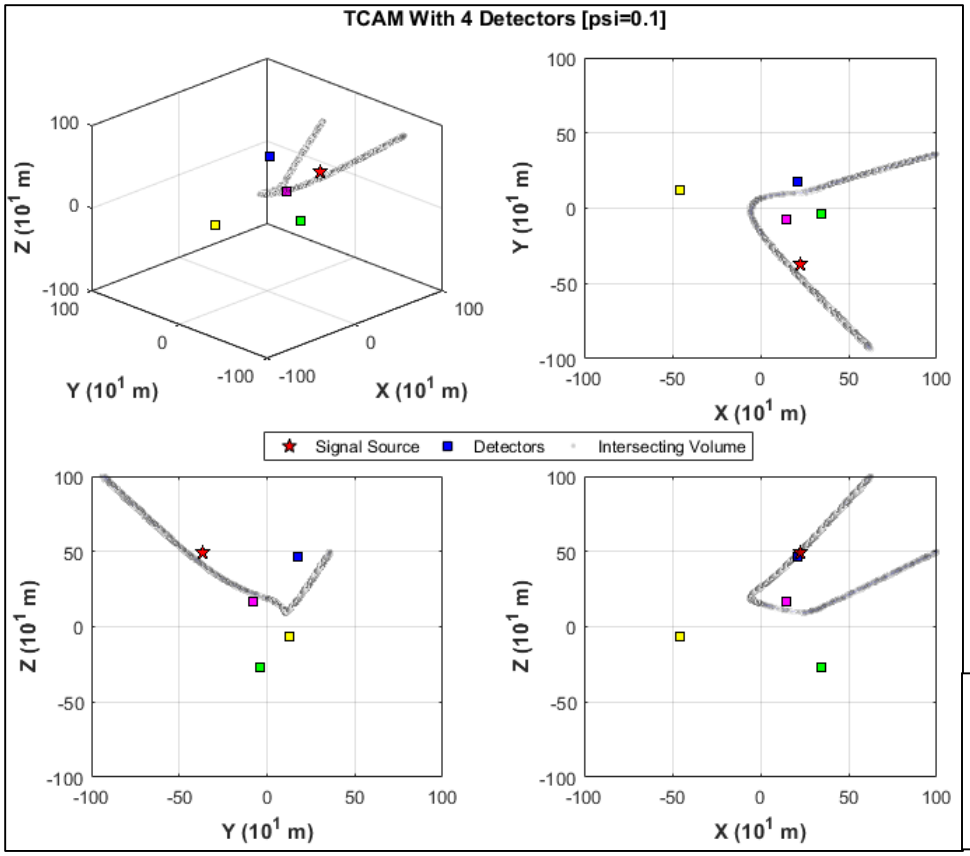

Figure 10:
TCAM results for 4 detectors, randomly situated, single pairing.

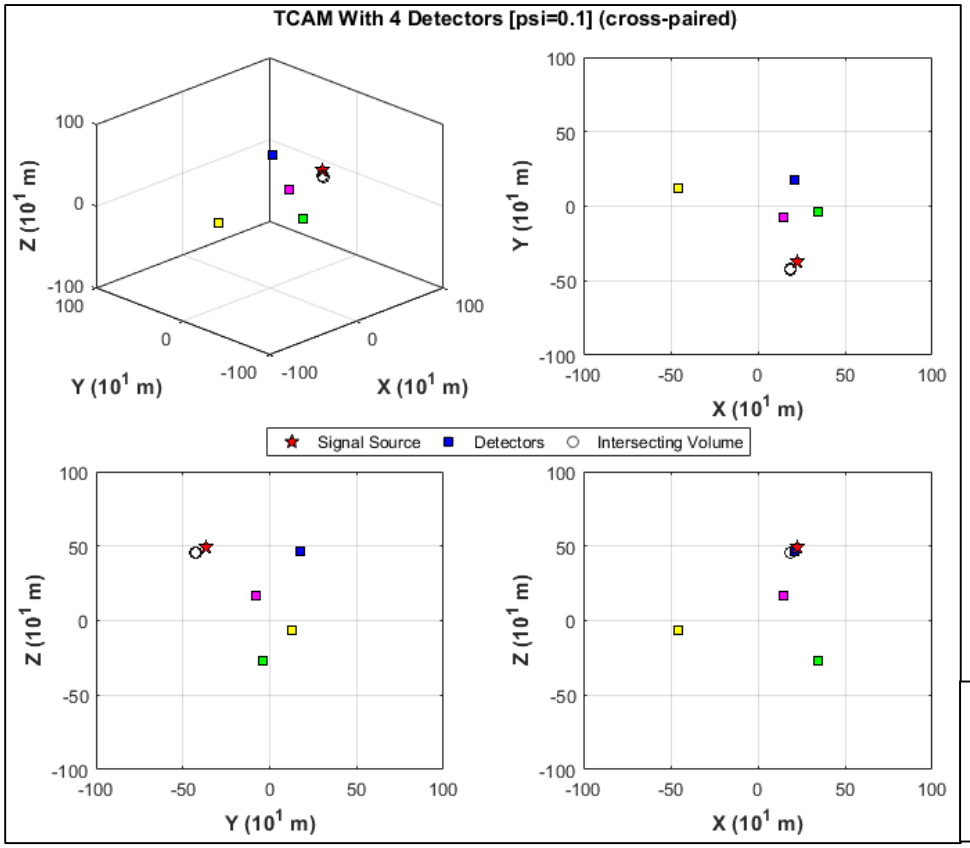

Figure 11:
TCAM results for 4 detectors, randomly situated, cross-pairing.

Unlike the detectors in figure 10 and figure 11, that were arranged randomly in the simulated space, the detectors in figure 12 are arranged in a fixed array that is comprised of two detector pairs with the same $\hat{z}$ orientation and equal spacing between all detectors. This produces a more uniform hyperbolic paraboloid toroidal volume that accurately contains the signal source location. Figure 12 offers a good visualization of how the intersection of two conic volumes makes the hyperbolic paraboloid toroidal shape as one conic region cuts a cross-section of the other to make a hollow bent ellipsoid.

The results of cross-pairing this same detector arrangement can be seen in figure 13. Once again cross pairing yields a much more precise localization of the signal source compared to the statically paired detectors. However, the localization results of the fixed detector array have more ambiguity than the randomly positioned detectors in figure 11. This is due to the sprawl of the detectors in figure 11 across the simulated space.

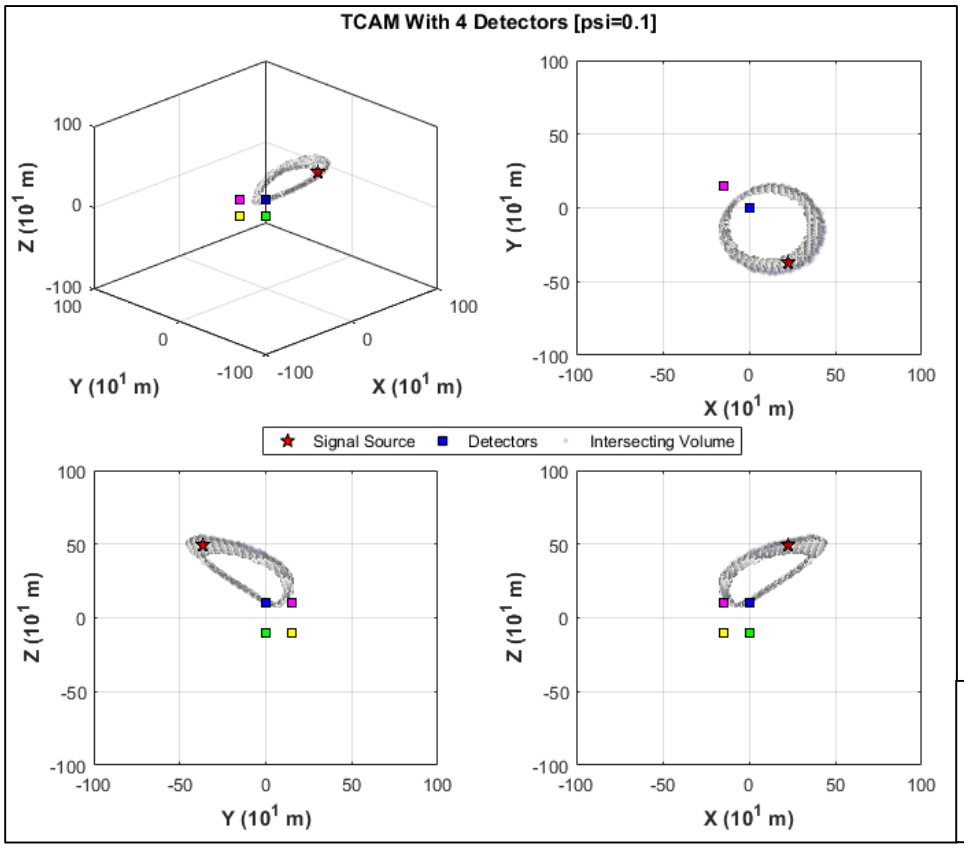

Figure 12:
TCAM results for 4 detectors, in fixed array, single pairing.

Localization with six detectors

The addition of a third pair of detectors, both randomly positioned and in a fixed array similar to figure 12, reduces the amount of ambiguity in the results. The shape of the intersecting volume of three detector pairs depends on the arrangement of the pairs. Figure 14 shows the results of randomly positioned detectors paired arbitrarily. In this case the intersecting volume is a tight narrow ellipsoid that is a precise and fairly accurate localization of the source; although the bulk of the intersecting volume is below the source location in the $-\hat{z}$ direction.

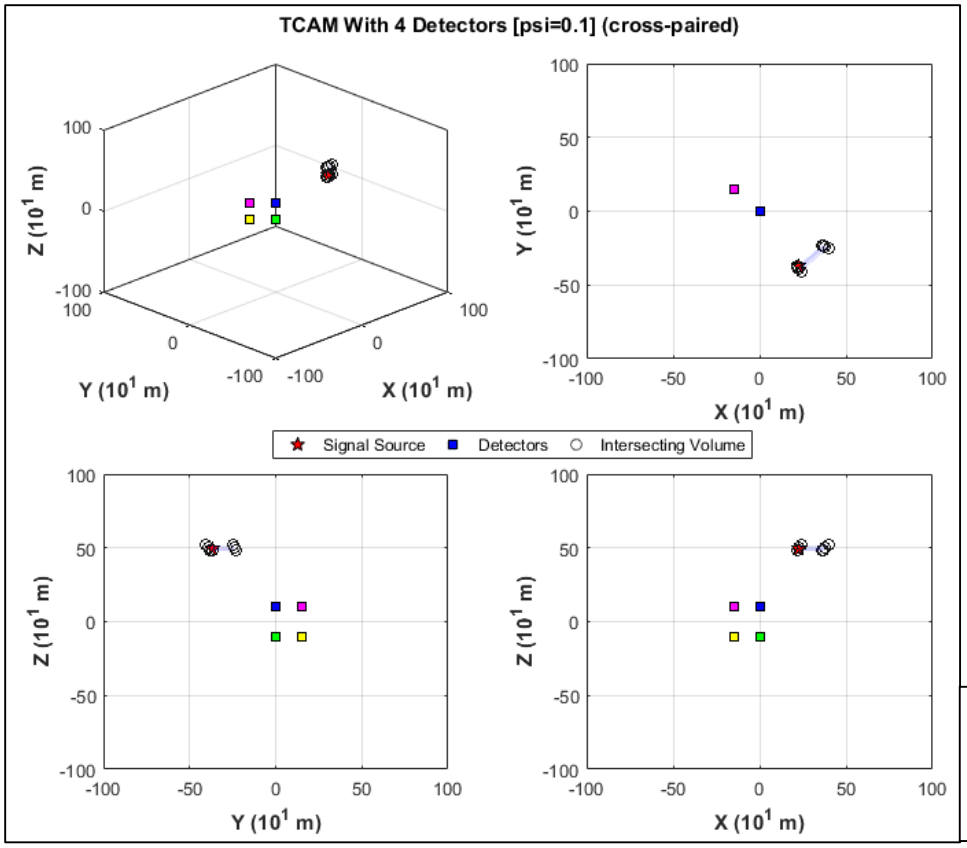

Figure 13:
TCAM results for 4 detectors, in fixed array, cross-pairing.

The accuracy of localization with six randomly situated detectors is greatly improved in figure 15 due to cross-pairing the detectors. Cross-pairing allowed for the analysis of fifteen conic regions instead of just three. The results seen in figure 15 are much more precise and accurate than in figure 14 even though the intersecting region is still slightly under the source location. Figure 16 and figure 17 show the results of having six detectors in a fixed array instead of randomly situated. The array layout is the same as basic configuration as previously used in the other examples, and the new detector pair was added as to make a triangular array of detector pairs that are paired vertically. As a side note, this array most closely emulates the hydrophone array used for the underwater acoustics experiments mentioned in chapter 1. The triangular array produces three conic regions with the same orientation in the $\hat{z}$ direction. The intersection of these three conic regions is usually scattered in several separate volumes, one of which contains the signal source location. These scattered results occur quite frequently when only three conic regions are being intersected; even if they are randomly situated. Figure 14's lack of scattering is coincidental from randomization of detector locations. Furthermore, cross-pairing the six detector array to make fifteen conic regions for analysis, as seen in figure 17, yields much more accurate results than the singly paired results of figure 16.

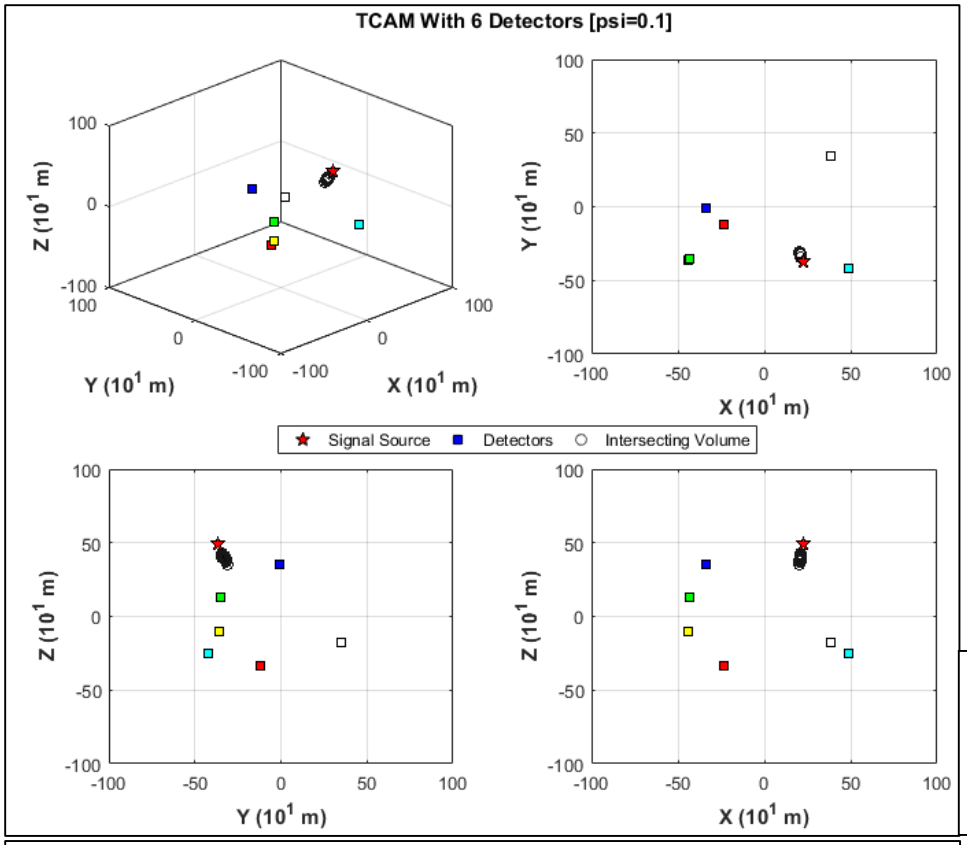

Figure 14:
TCAM results for 6 detectors, randomly situated, single pairing.

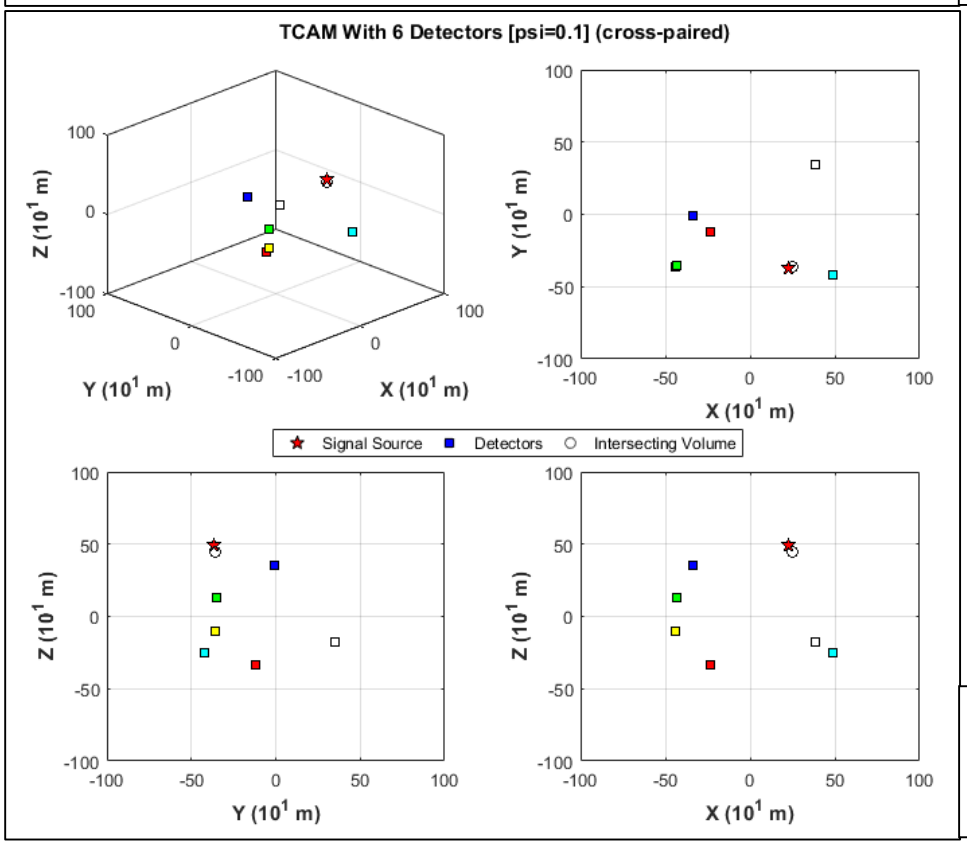

Figure 15:
TCAM results for 6 detectors, randomly situated, cross-pairing.

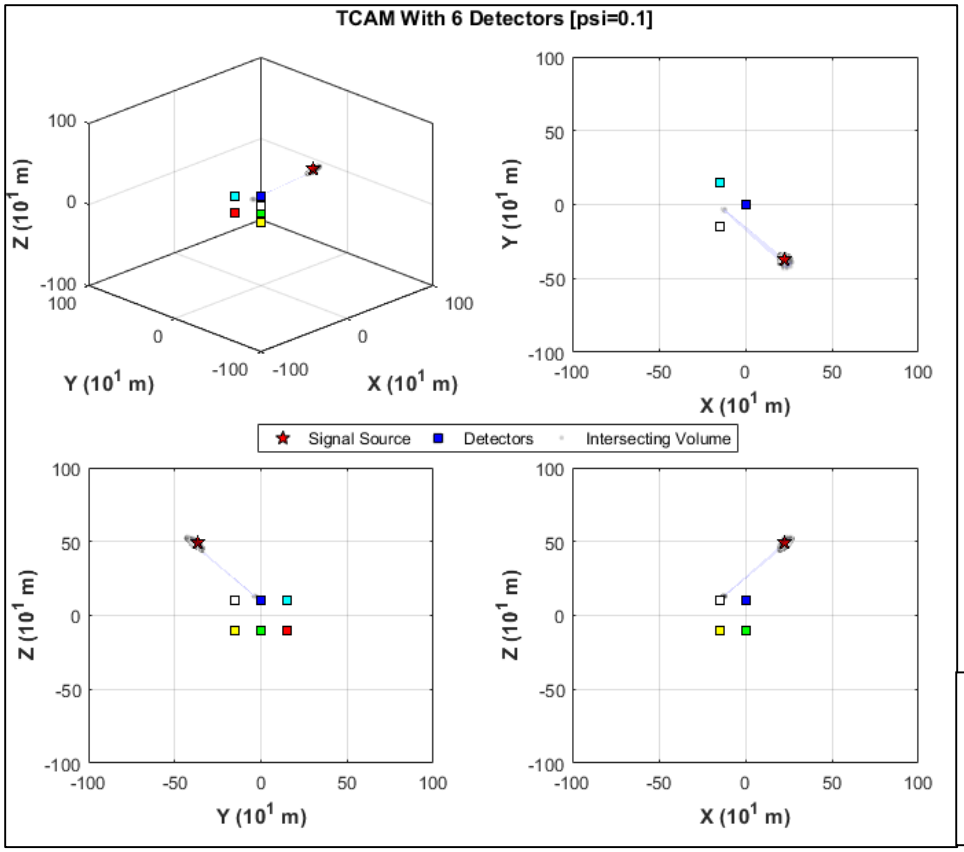

Figure 16:
TCAM results for 6 detectors, in fixed array, single pairing.

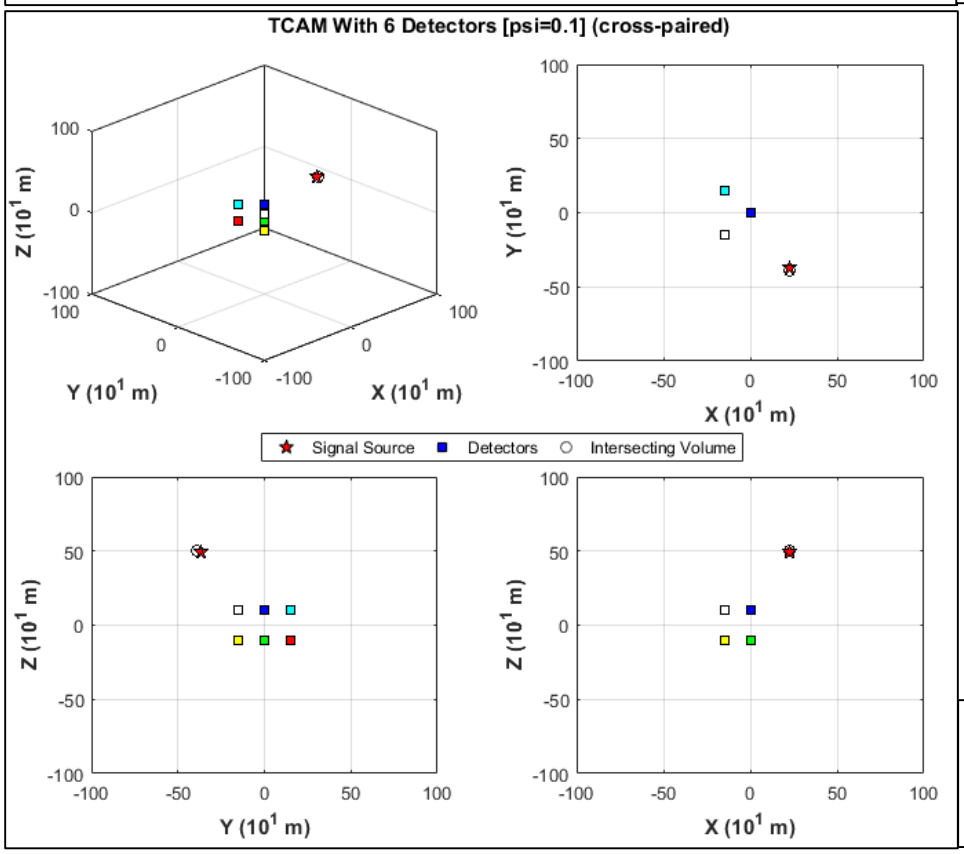

Figure 17:
TCAM results for 6 detectors, in fixed array, cross-pairing.

Localization with eight detectors

Finally, another pair of detectors is added to the cluster to show the results of localizing with eight detectors total. Once again, the detectors are situated both randomly and in a fixed array, and they are analyzed with both single pairing and cross-pairing. While the logistics of having eight synchronized detectors in a single observation region is unlikely in underwater acoustics, the results are presented for conceptualization of the TCAM technique with a multitude of detectors. The results of the randomly situated, single-paired, detectors are seen in figure 18. The sprawl of the detectors in figure 18 is fairly vast across the simulated space, and the resultant localization has high accuracy and precision. In fact, the localization results in figure 18 are nearly perfect. However, the results of cross-pairing the randomly situated detector in figure 19 yields a less accurate localization. This is an example of the dangers of cross-pairing detectors, especially detectors that are randomly situated. Granted, the accuracy of the cross-paired detectors is still considerably high in figure 19, but it is still not as accurate when compared to figure 18. The most likely explanation for the reduced accuracy in the cross-paired results is the tight clustering of some of the detectors in the set.

Arranging the detectors in an array similar to the ones used in previous examples, as seen in figure 20, produced nearly identical results to the six detector array in figure 16. The fourth detector pair was added to the prior triangular array as to make a diamond or box array. Once again the results in figure 20 show a scattered intersecting region that accurately contains the signal source location. Furthermore, the results of cross-pairing the detectors in the array, as seen in figure 21, is nearly identical to the results of cross-pairing the six detectors in figure 17.

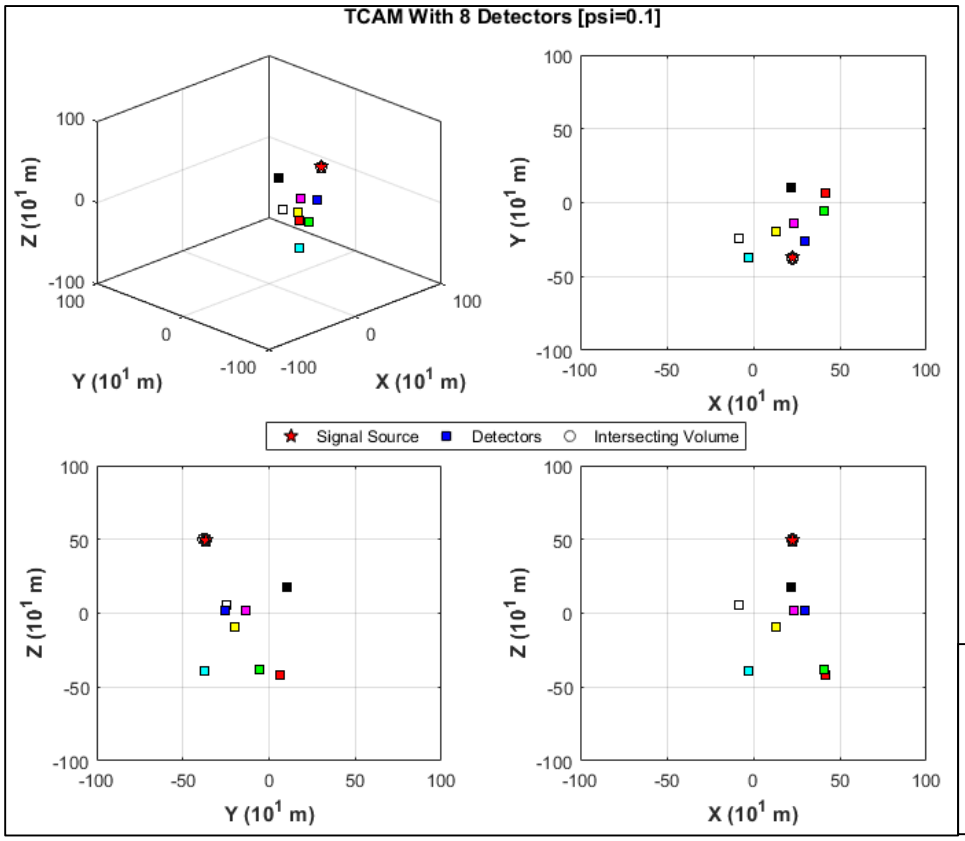

Figure 18:
TCAM results for 8 detectors, randomly situated, single pairing.

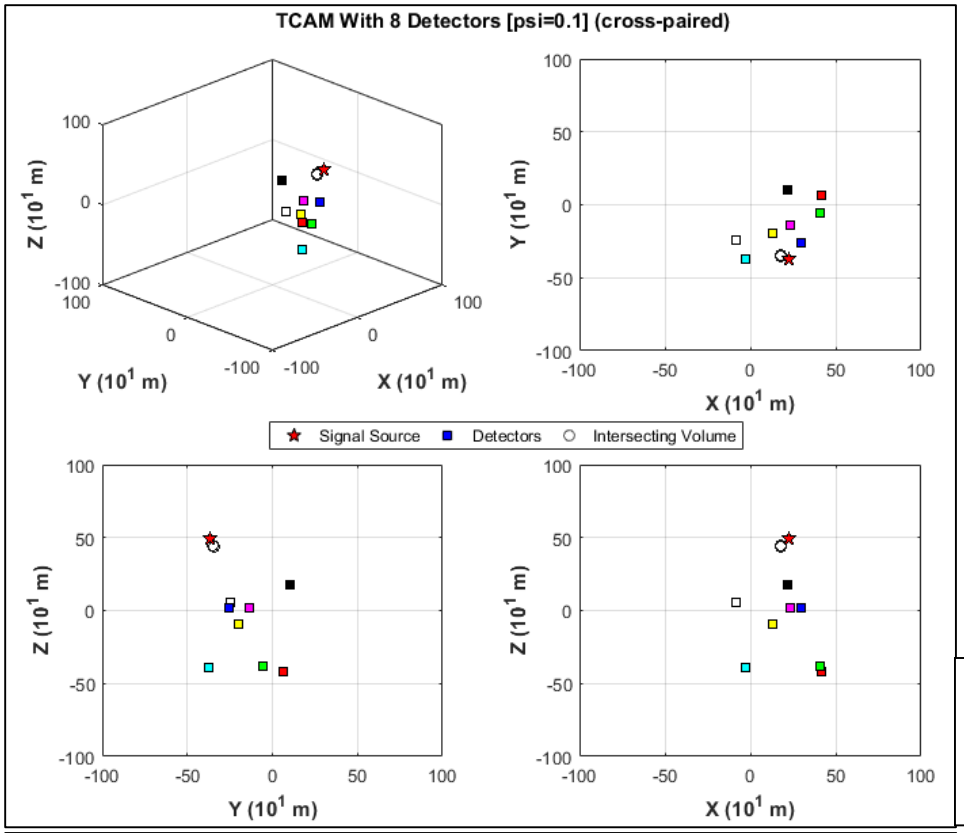

Figure 19:
TCAM results for 8 detectors, randomly situated, cross-pairing.

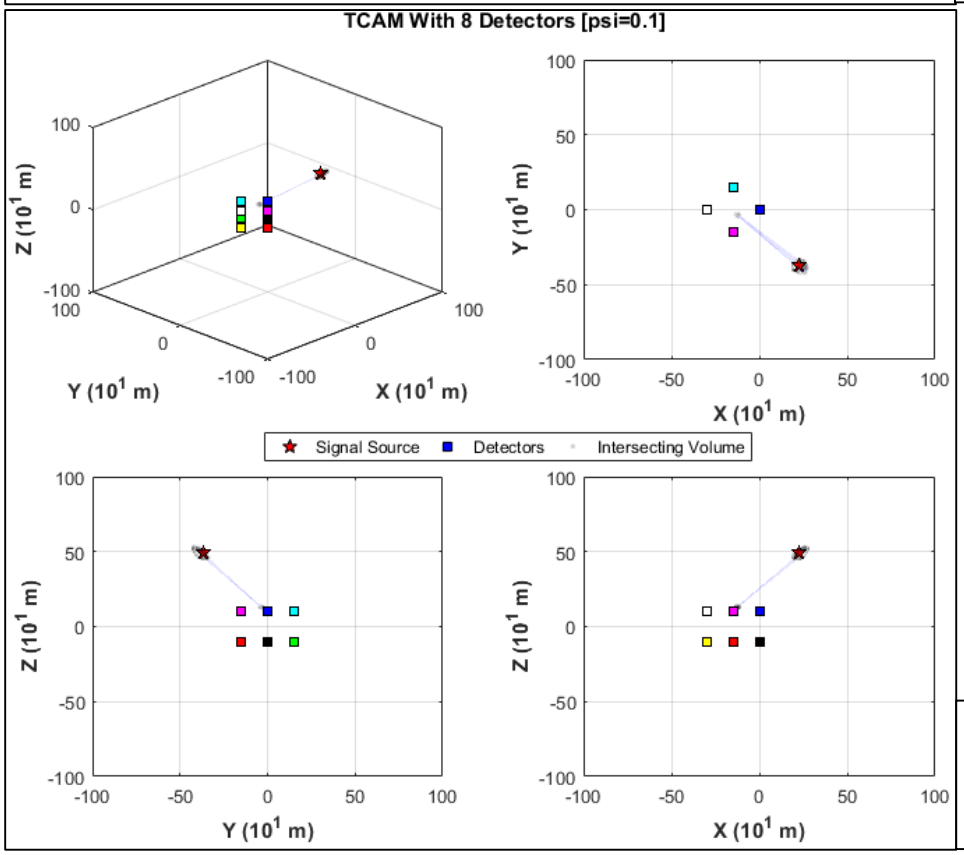

Figure 20:
TCAM results for 8 detectors, in fixed array, single pairing.

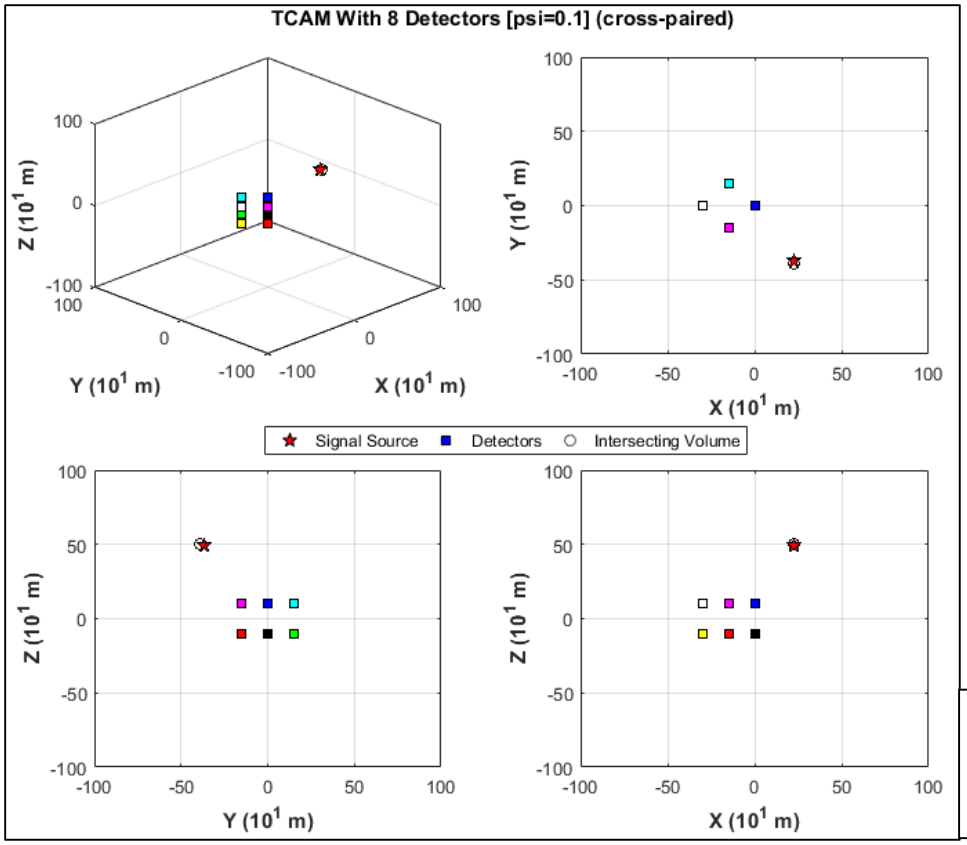

Figure 21:
TCAM results for 8 detectors, in fixed array, cross-pairing.

Chapter 4: Discussion and Conclusions

In summary, TCAM is a three dimensional wave localization technique for single path wave detections with unknown starting conditions. TCAM utilizes the TAZA model to approximate the zenith angle of incidence for pairs of detectors located throughout space. TAZA is a model for the relationship between the TDOA and the zenith angle of incidence from the center of the detector pair to the source of the detected wave. The TAZA angle defines the conic surface of probability on which the wave source is located. The conic surface of probability is expanded into a conic region of probability defined between the upper and lower bounds of the detection. The intersecting region of probability is the intersection of the detector pairs' conic regions of probability in which the signal source must be located.

Discussion

It can be seen from the results in chapter 3 that the TCAM technique offers a viable approach to three dimensional passive localization. The accuracy of TCAM depends on several different factors, but the number of contributing conic regions is the main factor that determines the accuracy of the results. As seen, more conic regions yield more accurate results.

Generally, one pair of detectors, therefore one conic region of probability, will produce an intersecting region that matches the conic region. Two pairs of detectors, therefore two conic regions, will typically produce the hyperbolic paraboloid toroidal shaped intersecting region. This shape is commonly non-uniform and can stretch across large areas of the region. Three detector pairs are the minimum number of pairs needed for TCAM to localize with high precision in three dimensions. The three detector pairs will likely produce a scattered ellipsoid shaped intersecting region, depending on the orientation of the detector pairs, but it can also produce singular results that are accurate and precise. Four detector pairs will usually produce a singular intersecting region, but as seen in figure 16, it can also produce a scattered region.

Cross-pairing the detectors proved to be a valuable tool that greatly increased the accuracy of localization. This was especially impactful in the examples with only a few detectors. The increased accuracy of cross-pairing the detectors is due to the increased number of conic regions contributing to the TCAM calculation. The increased number of conic regions offers redundant intersection calculations that hone in on the single source location. However, as stated previously and as shown in the results, cross-pairing can have a negative effect on localization accuracy depending on the orientation and position of the detectors. Furthermore, with increased conic regions comes increased computation for calculating the intersections of those regions. Thus cross-pairing can be extremely useful in the right situations and applications, but can also be a hindrance if the circumstances are unfavorable.

Future Work

The TCAM approach to localization is still in development with many aspects that can be optimized in the future. The goal is to make TCAM an easy to use and light weight tool that can perform on demand in a wide variety of signal localization applications. Focused areas of improvement include: reduced TAZA error, expedient calculation, spatial detector optimization, predictive tracking, and statistical probability analysis.

The main source of error in TCAM comes from the curve fitted expressions. The TAZA model was built from brute force computation of all possible TDoA in the local space. The resultant curve is fitted using the various expressions presented in this paper. As a result, the TAZA model expressions represent a balancing act between the number of coefficients needed for the expression and the error produced by the curve fit. Obviously more coefficients mean less error, but also more computation. Ideally, the optimal expression for TAZA would be symbolic with minimal coefficients and perfect accuracy. Expanding further on the spatial analysis done by Drysdale (Drysdale, 1924) may offer better expressions for TAZA in the near future.

The main drawback to TCAM, and for all passive localization techniques, is the time and cost of performing the calculations in a timely manner. TCAM has two computationally heavy parts that are difficult to calculate; the TAZA angle calculation and the intersecting region calculation. As previously stated, an ideal TAZA expression would eliminate the need for calculation of numerous coefficients in the expression. However, less ideal TAZA expressions are a viable option for the reduction of coefficients. Future work will not only look for the ideal expression for TAZA, but also for any expedient expressions that can simplify the calculations needed. The complexity of calculating of the intersecting region of probability depends on the number of conic regions of probability contributing the calculation. Obviously more intersecting regions means lengthier calculations. However, there is more than one way to determine intersecting volumes, and the computation can be minimized by optimizing the calculation of the intersecting region. Development of faster intersection calculations will enable TCAM to be performed more quickly and easily.

Furthermore, future research could explore the possibility of ideal detector arrangements that complements TCAM. Spatial relations are paramount in the implementation of TCAM, and it stands to reason that careful selection of the detector arrangement may be able to further optimize the accuracy of the method. The examples given include fixed arrangements of the detectors, and it is indubitable that the layout of the arrangement effects the localization results. The arrangements used in the examples were more emulative of the experimental arrangement that the TCAM technique was developed under, and were not indicative of an optimized arrangement. One simple example of a detector arrangement that produces unique TCAM results is a simple six detector layout with each detector being equidistant from the reference point in the positive and negative direction of each major axis. This centralized cluster produces conic regions with a common vertex at the origin, and that open in the direction of each major axis. The resultant intersecting region of probability is a straight tubular volume that is pointed directly at the signal source from the reference point. This arrangement was conceptualized as a detector array mounted on a single station, such as a submarine or space shuttle, and is not optimized for TCAM; however, it illustrates the concept of optimizing the detector arrangement.

The TCAM technique can also be improved by modern methods of machine learning and clustering. More specifically, machine learning algorithms can be used to perform predictive tracking of signal sources over time. By categorizing and clustering the results of individual TCAM results in a mutual space, predictive models can be built for the behavior and destination of unique signal sources that are being tracked (Nasser, 2007). For example, in the case of marine mammal tracking, if a specific species of marine mammal is observed performing repeated behaviors, maybe it circles around before diving down, then the machine learning algorithm can predict the dive location when circling begins. This rough example illustrates the possibility that machine learning can bring to localization and tracking with TCAM.

Machine learning can also contribute to better statistical probability results in TCAM. Currently TCAM cannot reduce any ambiguity in the intersecting region of probability, and as stated, the probability of the signal source location is evenly distributed throughout the volume of the region of probability. However, machine learning may offer a method of redistributing the probability in the volume based on prior measurements. Fourier analysis (Bracewell,2000) and wavelet analysis (Strang and Nguyen,1997) could also provide further categorization techniques to improve the machine the learning's statistical capabilities. This could potentially improve precision in applications with few detectors or with a scattered intersecting region.

Overall, the TCAM technique is still in its infancy and looks forward a bright future of growth and development. Improvements to TCAM can benefit the research community by offering quick and easy localization of signals. As stated, there is still an abundance of research and development to be done to the method.

Conclusions

Development of TCAM throughout my graduate career has been an engaging and fulfilling experience. I started researching three dimensional passive localization and decided to develop a modern method that was both effective and easy. Modelling the relationship of the TDoA and the zenith angle of incidence into the TAZA model enables expedient determination of the zenith angle. The TAZA model is expressed in three different ways, each offering various levels of complexity and accuracy. The zenith angle and TAZA expression used define a conic region of probability that contains the signal source location. Analysis of the intersection of multiple conic regions of probability reduces the possible location of the signal source to the overlapping volume of intersection; thereby effectively localizing the signal source to the most probable region of origin. Simulation testing with synthetic data confirms the validity of the TCAM technique. Testing in this manner allowed for the strengths and weaknesses of TCAM to be examined and improved. Overall the results of this new technique are pleasantly accurate and effective for passive localization in three dimensions with unknown starting conditions.

References

Fourier, Joseph (1822). Théorie analytique de la chaleur. Firmin Didot Père et Fils: Paris.

Ohm, G., (1843). Uber die defintion des tones, nebst dara geknupfter theorie der sirene un ahnlicher tonbildender
vorrichtungen, Annal. Phys. und Chem. 59, 513-565.

Strutt J.W. (Lord Rayleigh) (1876). "On our perception of the direction of a source of sound," Proced. Music.
Assoc. 2, 75-84.

von Hornbostel, E.M. and Wertheimer, M. (1920), "Über die Wahrnehmung der Schallrichtung," Akademie der
Wissenschaften, 388-396.

Klemm, O. (1920). "Ueber den Einfluss des binauralen zeitunterschiedes aud de localisation," Arch. Ges.
Psychol. 40, 123-129.

C. V. Drysdale, *Submarine Signalling and the Transmission of Sound Through Water*, in C. V. Drysdale, et. al., The Mechanical Properties of Fluids (London: Blackie and Son, 1925).

Strang, G., & Nguyen, T. (1997). *Wavelets and filter banks*. Wellesley, MA: Wellesley - Cambridge Press.

Bracewell, R. N. (2000). *The Fourier transform and its applications*. Boston, MA: McGraw-Hill.

US Department of Commerce, National Oceanic and Atmospheric Administration. (2013). How far does light travel in the ocean? Retrieved August 24, 2017, from https://oceanservice.noaa.gov/facts/light_travel.html

Nasser M. Nasrabadi, "Pattern Recognition and Machine Learning," Journal of Electronic Imaging 16(4), 049901 (1 October 2007). https://doi.org/10.1117/1.2819119

Leucippus, Democritus, C.C.W. Taylor. *The Atomists, Leucippus and Democritus: Fragments: a Text and Translation with a Commentary*. University of Toronto Press, 2010.

Appendix

Coefficient values for a_n (eq. 05)

n	0	1	2	3	4	5
$value$	2.78E+13	-1.5E+14	2.75E+14	-7.3E+13	-2.4E+14	-2.2E+13
n	6	7	8	9	10	11
$value$	5.02E+14	-3.1E+14	-5E+13	-2.5E+13	2.28E+13	5.06E+13
n	12	13	14	15	16	17
$value$	4.59E+13	-4.8E+12	-3.2E+13	-5.5E+13	-7.5E+12	3.26E+13
n	18	19	20	21	22	23
$value$	4.12E+13	1.54E+13	-2.9E+13	-2.4E+13	-2.8E+13	2.58E+13
n	24	25	26	27	28	29
$value$	3.8E+13	-2.8E+12	-1.4E+13	-3.8E+13	2.59E+13	1.5E+13
n	30	31	32	33	34	35
$value$	9.1E+11	-1.3E+13	-9.1E+12	1.22E+13	7.74E+12	-1.2E+13
n	36	37	38	39	40	41
$value$	-3.7E+12	1.47E+13	-1.3E+13	7.02E+12	-2.5E+12	6.54E+11
n	42	43	44	45	46	47
$value$	-1.2E+11	1.69E+10	-1.7E+09	1.15E+08	-5284825	151834.8
n	48	49	50			
$value$	-2427.19	74.86819	-0.03607			

Vita

Britt Aguda was born and raised in New Orleans, Louisiana. He received his bachelor's degree in Physics from the University of New Orleans in 2016. Mr. Aguda decided to continue his education at the University of New Orleans and enrolled in the MSAP program following his graduation. He joined the research group of Dr. Juliette Ioup, who was working with the LADC-GEMM Consortium with underwater acoustic data collected in the northern Gulf of Mexico. This thesis is a portion of the work Mr. Aguda accomplished in the field of acoustic localization. He plans to continue at UNO and work toward a Ph.D.